Highly Accelerated Test Method for Characterizing Likelihood of Breakdown in HVDC Dielectric Materials

Allen Andersen and JR Dennison
Utah State University Dept. of Physics
4415 Old Main Hill
Logan, UT 84322-4415, USA

ABSTRACT

Increasing application and development of HVDC technologies emphasizes the need for improved characterization of candidate insulating materials. Accurately predicting the lifetime to breakdown of dielectric materials by means of accelerated voltage step-up to breakdown tests can be prohibitively time consuming. Step-up to breakdown tests with sufficiently slow voltage ramp rates that continuously monitor leakage current have detected a distribution of DC partial discharge (DCPD) events occurring prior to breakdown, which increase with increasing field. These DCPD distributions are shown to correlate strongly with the likelihood of breakdown for four common polymers. Given that hundreds of DCPD events are typically observed in a single destructive, low-ramp rate, step-up test, measuring the distribution of the DCPD can potentially accelerate the characterization of the breakdown likelihood in candidate insulators by orders of magnitude in time. This relationship is discussed in the context of a dual-defect model of breakdown and thermally recoverable defects.

Index Terms—**Dielectric breakdown, HVDC insulators, partial discharges, testing.**

1 INTRODUCTION

THE present growth of HVDC technologies has resulted in increased interest in the improved characterization and diagnostic of HVDC insulation components [1, 2]. Indeed, despite decades of research, characterization methods and theoretical descriptions of the aging of insulators for HVDC applications lack the sophistication and utility of AC partial discharge diagnostic tools [2-6]. In this paper, we present evidence for a highly accelerated test method for characterizing the probability distribution of dielectric breakdown of solid insulators under increasing HVDC stress.

Accurately determining the breakdown threshold field for materials can be arduous due to the destructive nature of tests, the stochastic distribution of breakdown events, and the necessity of relying on accelerated test methods [7]. Measurements are presented here for four common polymeric insulators—low-density polyethylene (LDPE), polyimide (PI), biaxially oriented polypropylene (BOPP), and polyether ether ketone (PEEK)—showing that the distributions of DC partial discharges (DCPD) are strongly correlated to the distributions of breakdown events. As many DCPD events occur in each destructive breakdown step-up test, it is much easier to acquire large DCPD data sets, which results in accelerated material testing.

In this paper, we discuss our experimental methods and describe in detail the unique nature of the observed DCPD phenomena. Quantitative statistical assessments of heuristic evidence for how well the distributions of DCPD are correlated to the distributions of breakdown events are then presented. Finally, a theoretical dual-defect model is discussed, not as crucial evidence for the empirically established link between DCPD and breakdown, but as a candidate physical model for this relationship.

2 MEASUREMENTS

2.1 MEASUREMENT METHODS

The Utah State University (USU) Materials Physics Group (MPG) uses a modified ASTM parallel-plate configuration to perform voltage step-up to breakdown tests of insulating films [8, 9]. Extensive details of the USU experimentation have been published previously [10]. The two most significant modifications to standard test methods [8] are: (i) continuous monitoring of low-level leakage current, rather than use of a simple fuse or breaker; and (ii) stepwise voltage ramp rates (20 V every 4 s or average rate of 5 V/s), which is only 1% of the recommended maximum rate of 500 V/s. Voltages were incremented until complete breakdown occurred or up to a maximum of >600 MV/m at >15 kV. Currents were measured with low-resolution Amprobe® ammeters (~10 nA sensitivity) every 4 s; the meters measured average current over a ~0.5 s acquisition period with a duty cycle of ~12%. Use of a multiple electrode test fixture allowed measurement of six destructive step-up tests to be completed in ~6 hr, including time for sample configuration and vacuum pump down. Samples were clamped between a grounded metal sample

Manuscript received on 22 March 2017, in final form XX Month 2017.

mounting plate and six highly polished (<200 nm rms surface roughness) Cu high voltage electrodes, using a spring clamping mechanism to apply uniform sample contact pressure of ~0.4 MPa, in compliance with standard methods [8]. High temperature tests up to ~360 K with about ±2 K stability were accomplished by resistive heating of the entire test chamber. Cooling temperature tests down to ~135 K with about ±3 K stability were accomplished using a standard chiller to flow refrigerant through a cryogen reservoir thermally linked to the sample plate.

The data presented in this study include 148 destructive step-up tests of LDPE, 49 tests of PI, 56 tests of BOPP, and 84 tests of PEEK. Well-characterized, high-uniformity polymer samples from Goodfellow were used for all tests. LDPE samples (ASTM D-5213 type I [11]) tested had measured thicknesses of 29.6 μm ±0.7%, density of 0.92±0.01 g/cm^3 [12], estimated crystallinity of 50% [13], a peak fractional mass distribution of ~$6{\cdot}10^3$ amu [14, 15], and a relative dielectric permeability of 2.26 [12]. Kapton HN samples of PI (ASTM D-5213 type I [11]) had measured thicknesses of 25.0 μm ± 2%, density of 1.43±0.01 g/cm^3 [16], and a relative dielectric permeability of 3.5 [16]. BOPP samples tested had measured thicknesses of 27.6 μm ± 1%, density of 0.90±0.05 g/cm^3 [17], and a relative dielectric permeability of 2.4±0.2 [17]. PEEK samples had measured thicknesses of 29.6 μm ± 1%, density of 1.26±0.005 g/cm^3 [18], and a relative dielectric permeability of 3.25±0.05 [18]. All samples were chemically cleaned with methanol prior to a bakeout at ~385±5 K (338±3 K for LDPE) under <10^{-3} Pa vacuum for ~72 hr while in contact with a grounded surface, to eliminate absorbed water and volatile contaminants and any residual stored charge [14]. Nominal breakdown field strengths for unbaked samples using standard ASTM 149 test methods were listed as 200 MV/m for LDPE [13], 303 MV/m for PI [16], 110-150 MV/m for BOPP [17], and 200 MV/m for PEEK, respectively.

2.2 OBSERVED FEATURES IN I-V CURVES

Current can be measured with increasing voltage to accurately identify the breakdown field strength, using an enhanced operational definition of dielectric breakdown for DC voltage step-up tests [19]. Figure 1 indicates features observed in typical step-up test I-V curves with labels **A** through **E**, including those seen frequently only in test systems that measure lower currents and use slower voltage ramp rates. These additional features are often accentuated in log current versus applied voltage curves, such as Fig. 1(b).

At the simplest level, dielectric breakdown is indicated by a transition from negligible currents to a:

A. *Post-breakdown ohmic current* with slope determined by the current limiting resistors in the test circuit. See both Figs. 1 (a) and 1(b).

For typical step-up tests in the USU system, for insulating materials with >10^{16} Ω-cm steady leakage currents of <10^{-8} A are expected as applied voltages are increased until breakdown, which is marked by a transition to linearly increasing ohmic currents of >10^{-5} A determined by two 100

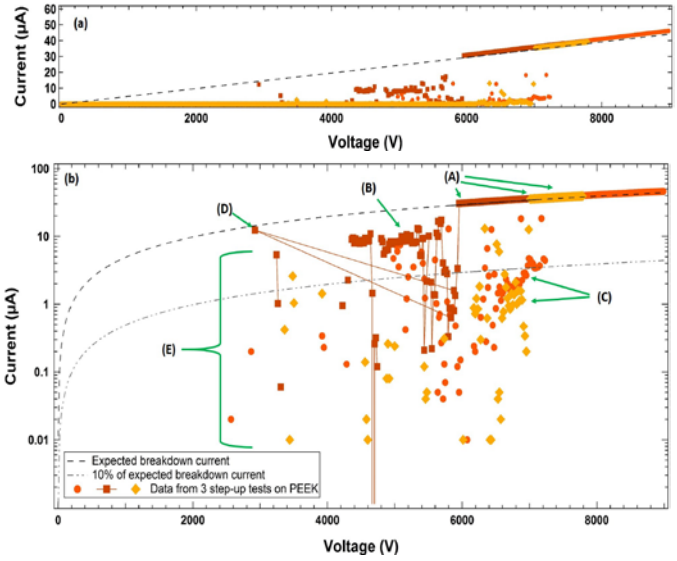

Figure 1. Examples of current traces from three voltage step-up tests on PEEK films together with the expected breakdown current (dashed lines) and 10% of the breakdown current (dot-dashed lines) are shown or reference. (a) Linear I-V plot. (b) Semi-logarithmic IV plot. Plot features are indicated as: (**A**) Dielectric breakdown marked by transition to a linear ohmic slope corresponding to the circuit's current limiting resistors; (**B**) Dielectric breakdown with some residual resistance; (**C**) Field-enhanced conductivity; (**D**) Surface flashover; and (**E**) DCPD.

MΩ current limiting resistors in series with the sample. For most highly insulating materials tested, the leakage current below breakdown is below the sensitivity of the ammeters, as seen in Fig. 1(a). Such low leakage currents, as low as 10^{-16} A are routinely observed for such materials in high sensitivity constant voltage conductivity test systems [14, 20, 21].

Two related features, which exhibit monotonically increasing current with increasing voltage, well above current sensitivity, are sometimes observed consistently in specific materials:

B. *Dielectric breakdown with significant residual resistance.* This current steadily increases in an ohmic fashion, but with more resistance than expected. See Fig. 1(b); also see [22]. This is interpreted as a partial breakdown of the material with residual sample resistance comparable to the current limiting resistances, perhaps through only a fraction of the sample thickness. Even in cases when there is no transition to *Post-breakdown ohmic current*, after the test there is visible evidence of breakdown on the sample surface, indistinguishable from the damage observed for full breakdowns.

C. *Field-enhanced conductivity.* Many consecutive current measurements increase super-linearly with voltage, at higher voltages near breakdown. See Fig 1(b); also see [23]. This is attributed to field-enhanced dark current conductivity, which usually occurs at fields above 30% of nominal breakdown [14]. Such currents rarely exceed 10% of the expected breakdown current [13].

On rare occasions, breakdowns and transitions to ohmic behavior are observed at very low voltages for a specific sample of a material. After these tests, there is visible

evidence of breakdown on the sample surface. These features are attributed to sample imperfections or damage to the sample surface; often there is clear evidence in images of the specific sample either before or after the breakdown test showing these sample defects.

Further, most low-ramp-rate step-up tests performed with the USU system—including all those reported here—exhibit additional transient current features in breakdown I-V curves, most often with only a single sequential current measurement above the leakage current or current sensitivity level. One such feature is:

D. *Surface flashover*. Occasionally, a sudden (often large) voltage drop is measured together with current corresponding to the ohmic current at this reduced voltage. See Fig 1(b). This is interpreted as a brief surface flashover, where current temporarily bypasses the shorted test sample in the circuit. On several occasions at which surface flashover features were observed in the I-V curves, there were features observed on the surface indicating arcing at the edges of the samples.

On very infrequent occasions, very large transient currents are observed, well above the ohmic breakdown curve (see for example, Fig. 5 in [23]). These are attributed to instrumentation malfunctions, such as erroneous readings by the current or voltmeters or the data acquisition card.

By far the most frequent transient current features are those we classify as *DC Partial Discharges* (DCPD), labeled **E** in Fig. 1(b). We have referred to these DCPD traces as pre-breakdown arcing in previous papers [24, 25]. A standard PD monitor is not typically used for the voltage step-up tests shown here. Nevertheless, we can clearly distinguish DCPD from other transient features discussed above. No visible damage to the sample has been observed in tests with DCPD which were terminated prior to breakdown. On average, more than 10 DCPD traces of varying amplitude are observed in a single step-up run. Although these DCPD features can be observed in successive current measurements (particularly at voltage approaching the breakdown voltage), they generally are distinct, single measurements of current that return to the background or field-enhanced conductivity levels for subsequent current measurements. The onset and frequency of these DCPD vary significantly from material to material of the same sample geometry indicating that they depend on the sample material rather than being an artifact of the test apparatus. The easy identification of surface discharges (see **D**) indicate that DCPD traces must be a bulk phenomenon. Such surface discharge traces are found to be very infrequent at low pressures $<10^{-3}$ Pa where MPG measurements are typically made, and to increase in frequency more than an order of magnitude as pressure is increased to $\sim10^{0}$ Pa where Paschen discharge is more likely to occur.

DCPD measured with slow ammeters are more frequent and of higher current amplitude at higher applied fields. Observed DCPD transient current features ranged over two orders of magnitude in current below the breakdown current.

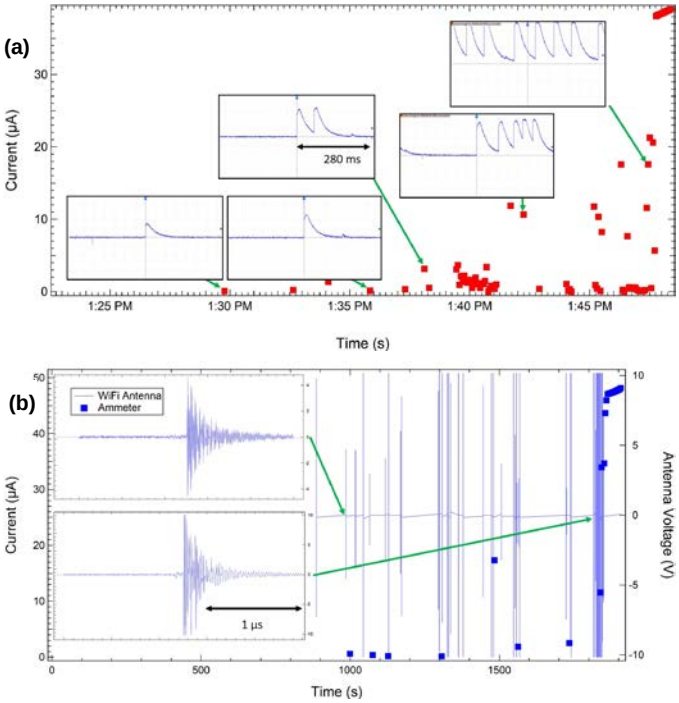

Figure 2. Supplementary measurements of DCPD in voltage step-up tests. **(a)** DCPD events from a step-up to breakdown test in PI. In-line shunt resistor oscilloscope traces of DCPD were correlated to DCPD as seen by the standard ammeter; five of these are shown here. Large amplitude ammeter events correspond to many DCPD of similar amplitude as seen by the oscilloscope. **(b)** DCPD measured during a voltage step-up test on BOPP by a 2.4 GHz WiFi antenna connected to a 50 Ω load oscilloscope shunt, together with the standard ammeter curve. The inset shows to examples of individual trigger events. As in (a), larger amplitude ammeter traces correspond to multiple DCPD as seen by the antenna.

To investigate these DCPD with greater time resolution, two additional methods have been employed. First, the test setup was modified to include a 100 MHz oscilloscope (Tektronix TBS 2000 Series) measuring voltage across a 10 kΩ shunt resistor in series with the ESD circuit between the ~200 MΩ current limiting resistors and ammeter. Current was monitored as usual at ~2 Hz with the Amprobe® ammeter and at ~10 kHz with the oscilloscope, and the data from both instruments were correlated in time. The decay time for each DCPD is limited by the RC time constant of the measurement circuit (approximately 40 ms). An example of these measurements is shown in Fig. 2 (a). All DCPD seen with the in-line method (Fig. 2 (a)) were on the same order of magnitude ($\sim10^{-5}$ A peak current).

The second DCPD supplementary detection technique used was the common RF antenna PD detection method [26-28]. The short time scale of individual DCPD result in a broad frequency-space signal, and detection antennas cited in the literature observe frequencies from 1 MHz to 5 GHz [26-28]. HVAC partial discharge testing is not performed in our laboratory, which is not yet equipped with an off-the-shelf PD monitor typically used for most HVAC and HVDC partial discharge tests performed in other labs [29]. However, ubiquitous 2.4 GHz WiFi antennas fall within the range of typically used DCPD detection antennas. A 2.4 GHz WiFi antenna, placed adjacent to a vacuum chamber glass window,

was connected to a 50 Ω load and monitored using an oscilloscope (Tektronix TDS 2014) and custom LabVIEW data acquisition software. An example of these measurements is shown in Fig. 2 (b). The insets of Fig. 2(b) show example traces of individual events decaying over hundreds of ns. Significant ringing in the signal is likely due to impedance mismatch in the rudimentary setup. Although each DCPD recorded by the ammeter has corresponding antenna measurements, some DCPD are not observed by the ammeter due to its ~12% duty cycle. Large-amplitude ammeter events correspond to multiple antenna measurements. This is especially apparent immediately prior to breakdown.

While both in-line and antenna measurements show measurable variation between individual DCPD, they do not cascade orders of magnitude in amplitude as recorded by the slow ammeter. These independent measurements demonstrate that the larger current values measured by the ammeter result from integrating over multiple fast higher amplitude DCPD of about the same magnitude. Therefore, a correction for the measured arc count is needed to correct for multiple short-duration DCPD events integrated and averaged within a single ~0.5 s ammeter data-acquisition interval. The estimated ammeter time-averaged amplitude of a single DCPD is ~0.1 µA. For the statistical analysis of DCPD events presented below, the arcing rates measured with the ammeter have been corrected for these multiple arcs per acquisition time by estimating the number of single DCPD events in higher-current traces as the measured current divided by this average single DCPD current. This correction recovers the result observed by the independent fast time resolution measurements of ~10^2 DCPD observed in a typical MPG test.

Let us return to a discussion of DCPD as observed in voltage step-up tests without supplementary DCPD detection equipment. As shown in Fig. 3 (a), the frequency of the DCPD increase substantially with increasing voltage. For all four materials studied, no DCPD were observed below a threshold voltage. It may be that the apparent threshold is simply a consequence of the fact that the observed rates at threshold voltages predict at most a few DCPD per run.

Fig. 3 (b) shows the estimated DCPD count rate for LDPE and BOPP as a function of voltage ramp rate, given various instrument duty cycles. This count rate is estimated as the product of the average DCPD frequency above DCPD inception, the duty cycle, and duration of a test run (estimated as the ratio between the nominal breakdown voltage to the voltage ramp rate). The average estimated DCPD frequencies above inception for each material in Fig. 3 (a) are 4.7 ± 0.3 Hz for BOPP, 1.35 ± 0.09 Hz for PI, 0.86 ± 0.04 Hz for LDPE, and 0.54 ± 0.05 Hz for PEEK.

The distribution of these DCPD features with applied voltage are clearly stocasitic in nature and vary significantly from material to material, but are consistent for many different step-up tests on the same materials; again, this strongly suggests that DCPD features are clearly not experimental artifacts [24]. Further arguments of possible similarities in the origins of DCPD and DC breakdowns are discussed in terms of a proposed physics-based dual defect model in Section 4.

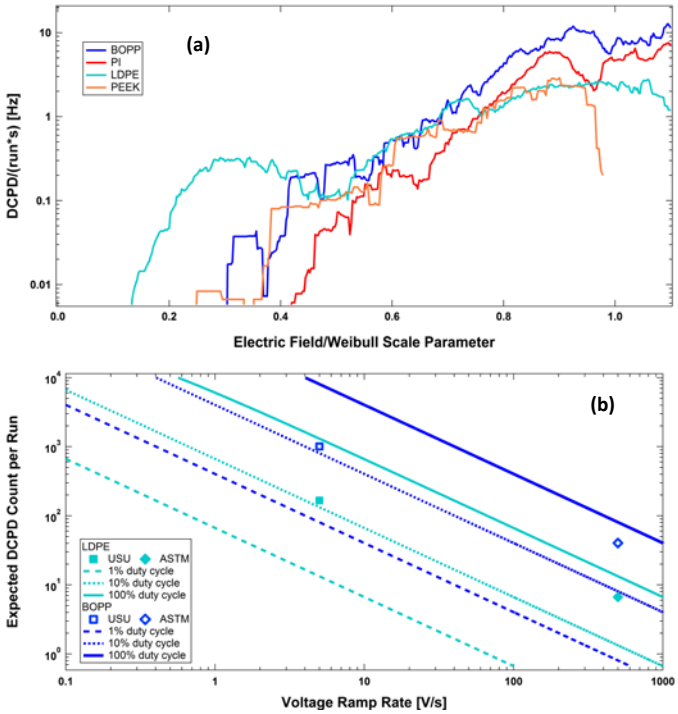

Figure 3. (a) Estimated frequency of DCPD from data versus applied field scaled by breakdown field, corrected for equipment duty cycle and smoothed with a 500 V boxcar method. (b) Estimated DCPD count measurement for various duty cycles versus voltage ramp rate. Upper blue curves correspond to the material with the highest average DCPD frequency, BOPP. The lower cyan curves represent the estimates for LDPE. Square markers indicate the estimates using the USU ramp rate and duty cycle (~12%) for BOPP while diamond markers indicate estimates of the ASTM method with a 500 V/s ramp rate and a 50% duty cycle.

In past publications, we have commented as to why DCPD are not frequently reported in similar test set-ups [23, 25]. We again summarize and expand these arguments. Perhaps the primary reason DCPD are seldom reported with voltage step-up to breakdown tests is that they were not the usual target of such measurements. We have noted a 2015 breakdown study where small current traces similar to what we describe here were reported as a side note to the primary results [30]. Most importantly, these factors are:

(i) Continuous monitoring of leakage current. The standard procedure for step-up to breakdown tests recommends the use of a fuse or breaker to indicate breakdown [8]. If leakage current is not monitored continuously then it will be extremely unlikely that DCPD will be observed [19]. At most, if the current sensing element has a low tripping threshold, DCPD would result in a false positive in the dielectric breakdown test. Likewise, as shown in Fig. 3 (b), setups with poor duty cycles may also struggle to observe DCPD. Likewise, as shown in Fig. 3 (b), setups with poor current sensor duty cycles may also struggle to observe DCPD

(ii) The use of slower ramp rates than most standard tests [8]. As shown in Fig. 3 (b), the estimated DCPD count decreases dramatically with increasing voltage ramp rate. MPG step-up tests, with an average voltage ramp rate of 5 V/s, are likely to see 100 times more DCPD events than

using a 500 V/s ramp in a given run. In LDPE, an average of 17 DCPD observations occurred (unadjusted for amplitude). At 500 V/s we would expect fewer than one in twenty tests to include even a single DCPD observation.

(iii) Ammeters used were sensitive down to 10 nA. Depending on the breakdown voltage in a given test, current through our test circuit at breakdown is limited to ~40 μA. With DCPD observations as small as ~0.1 μA, they might easily be missed by a setup exclusively designed to test for dielectric breakdown.

Other experimental techniques that may also contribute to our ability to observe DCPD include:

(iv) Stepwise ramping with sharp edges in the applied voltage profile used in these tests may trigger more DCPD than a continuous voltage ramp [31].

(v) Large flat electrode areas, rather than sharp needles often used in breakdown tests [32].

(vi) Beveled electrode edges that minimize edge effects [33].

(vii) Polished electrodes to minimize the effects of protrusions [34, 35].

(viii) Spring-loaded sample clamping system to maintain a uniform E field.

(ix) Samples that extend well beyond the electrode area to reduce surface flashover.

(x) High quality samples of uniform thickness, used to minimize impurities and associated erroneous breakdown.

(xi) Samples were baked prior to testing, to remove any absorbed water or other volatiles [34].

(xii) Tests were performed under high vacuum ($<10^{-3}$ Pa base pressure), rather than in oil or some other dielectric medium.

3 CORRELATION OF DCPD AND BREAKDOWNS DISTRIBUTIONS

The test setup used for these tests was not originally intended to measure DCPD. Initially, all of the phenomena described in Section 2.2 apart from breakdown were unanticipated and puzzling. Nevertheless, the similarities between breakdown and then-termed pre-breakdown arcing event distributions were too obvious to ignore.

Even without a clear understanding of the physical origins of pre-breakdown DCPD events, it became clear that if the distribution of breakdowns in test materials could be shown to be approximated well by the distribution of DCPD events versus applied field, this could greatly accelerate the characterization of the breakdown distributions and possible threshold field for materials tested.

3.1 BREAKDOWN DISTRIBUTIONS

The breakdown strength of a dielectric material is often listed in tables as a constant value, occasionally with a note that the value listed corresponds to a certain temperature or thickness [7]. This convenient representation can belie the stochastic nature of breakdown and that, even under ideal conditions, repeated tests result in a distribution of breakdowns with applied electric field (see black curve in Fig. 4). At first pass, the uninitiated might suggest reporting the average and standard deviation of breakdown voltages; however; Gaussian statistics are not applicable to failure statistics that need to account for the removal for samples from the test population once they have broken down [32].

Breakdown data are commonly fit to a two-parameter Weibull distribution, with the scale parameter corresponding to 63.21% likelihood of breakdown given as the nominal breakdown voltage [32, 33]. The Weibull shape parameter corresponds to the spread of the distribution, giving an estimation of the likelihood of breakdown at lower fields or the width of the distribution.

It is troubling to note that the standard recommended number of tests is only five [8]. When it is critical to estimate breakdown inception fields for long time to breakdown operation-like scenarios, such cursory measurements are obviously insufficient [7]. To better extrapolate to breakdown probabilities at low fields, larger data sets reveal that often more complicated distributions such as three-parameter or mixed Weibull distributions are more accurate [33, 36]. Static voltage endurance time tests (SVET) begin to directly probe the time to breakdown of dielectrics at a fixed applied field; however, these very time consuming tests also rely on extrapolation to estimate breakdown threshold fields that correspond to very long times required for HVDC applications or to determine if there is indeed a lower field threshold for breakdown [10].

3.2 ACCELERATED TESTING

The destructive nature of step-up to breakdown tests, particularly in the parallel plate configuration, results in a single datum per test. The prospect of accurately determining the distribution of breakdowns, especially the inception field where breakdowns are least likely to occur, becomes onerous. The popular test method of vapor-deposited electrodes on a large sample sheet allows for multiple breakdowns and increased data collection rates, but it has been shown that these events are not fully independent of each other [37].

If relevant, the numerous DCPD traces could uncover the threshold field with much less effort and expense. In a typical step-up to breakdown test, tens of DCPD traces, corresponding to hundreds of DCPD events, are commonly observed. For independent, random events relative uncertainty decreases as the inverse square of the root of the number of events. If the DCPD are related to dielectric breakdown, then it is clear that the number of tests needed to characterize the dielectric breakdown is greatly reduced, by at least an order of magnitude. Further, of critical importance is the breakdown threshold field. Non-destructive tests probing the distribution of DCPD well below expected breakdown fields could accelerate the characterization of this hard-to-test but critical inception behavior.

3.3 INITIAL ANALYSIS OF DCPD DISTRIBUTIONS

Our first attempt to investigate the existence of a connection between dielectric breakdown and DCPD compared Weibull

fits to the cumulative distribution of breakdown data to Gaussian fits to the probability density of DCPD data. This initial study was suggestive, though unsophisticated, and not entirely convincing [24].

The empirical cumulative distribution (ECD) estimates the probability of occurrence $\hat{P}$ of an event as a function of a variable (in our case electric field F) based on n data points x_i as

$$\hat{P}(F) = \frac{1}{n}\sum_{i=1}^{n} \mathbf{1}\{x_i \le F\} \quad \text{where}$$

$$\mathbf{1}\{x_i \le F\} = \begin{cases} 1 \text{ if } & x_i \le F \\ 0 & \text{otherwise} \end{cases} \qquad (1)$$

It is apparent that (1) is only a valid approximation of the true underlying cumulative probability distribution for large n.

Fig. 4 compares the ECD of 96 breakdown tests in LDPE to the ECD of the 46,057 discretized DCPD events from those same tests. It should be noted that in many voltage step-up tests there is very erratic behavior where the current changes greatly from one measurement to the next without returning to baseline current before clear breakdown occurs. When these traces are too erratic to distinguish between any of the cases described above, any DCPD therein are not countable [23]. This tends to occur at the higher fields just before breakdown so many DCPD are likely to be missed this way; therefore, we expect the distribution of DCPD to be somewhat distorted or shifted. This is evident in Fig. 4 and its inset.

Although the two ECDs in Fig. 4 appear to be similar, to compare two sample populations of different sizes to each other, a robust, non-parametrized statistical method was required.

3.4 COMPARISON OF EMPRICAL CUMMULATIVE DISTRIBUTIONS—QUANTILE-QUANTILE ANALYSIS

After further study and consultation with statisticians, we applied quantile-quantile (q-q) analysis to the problem. Q-q plots directly compare the cumulative distributions of two observables. Each point on a q-q plot represents values (in our case electric field) for which each observable has the same probability of occurrence. To briefly review q-q analysis it is convenient to begin with comparing ECD plots. In Fig. 4 the dashed lines show two examples of quantile matching. For an ECD plot, the y-axis represents the estimated probability of occurrence, or quantile. For each quantile Q_n, there is an x-axis value for each ECD plotted. These x-axis pairs for each Q_n become x- and y- values x_n and y_n on the q-q plot. For two samples of different sizes, some type of interpolation is necessary to get matching quantiles. Since there are many more DCPD than breakdowns, the quantiles of DCPD events were linearly interpolated to match the quantiles of the breakdowns.

If the underlying distributions are precisely the same, the q-q plot will follow a unitary linear relationship, namely $y = x$. Any other linear q-q plot demonstrates that the two distributions are indeed correlated, while q-q plots deviating

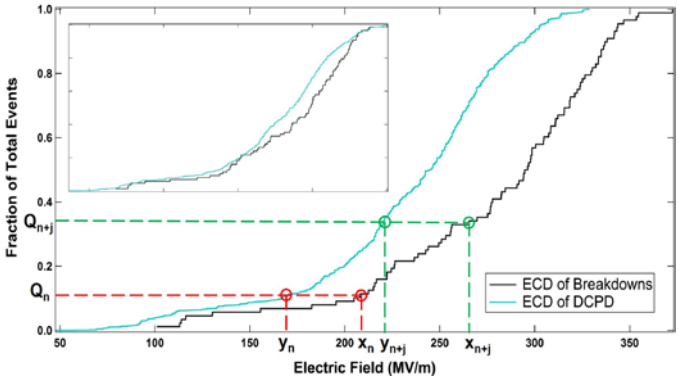

Figure 4. The empirical cumulative distributions (ECD) of breakdown and DCPD events from 96 voltage step-up to breakdown tests in LDPE at room temperature. The inset shows the ECDs normalized to the highest field value for each type. Red and green dashed lines show examples of matching quantiles from two ESDs. For two ESDs plotted together, one quantile—the y-axis value—corresponds to two x-axis values which become the (x,y) pairs on a q-q plot. The ECDs shown here yield the q-q plot Fig. 5 (a).

significantly from linearly show that the distributions are not correlated [38].

The advantage of the q-q plot method is that it results in a non-parametric plot that is easy to interpret qualitatively—if the distributions are correlated, the q-q plot will be linear; otherwise, it will not. The drawback is that for a two-sample q-q plot, quantifying the results becomes more complicated than a simple linear correlation, especially for a q-q plot comparing two data sets rather than a single data set to a known distribution function. Calculating a linear correlation coefficient gives artificially good results due to the sorting in (1) required when creating ECDs for the q-q plot, even for q-q plots that clearly deviate from linear. In our previous publication we erroneously used this method to determine the significance of the fit [25]. The methods that do exist, such as a two-sample Kolmogorov-Smirnov statistic or other methods, result in a confidence interval around the q-q plot that statistically gives a range of confidence of where the data actually are on the plot [39-41]. From the authors' perspective, such methods are not satisfying measures of the goodness or significance of the linear fit. For the purposes of this study, we contrast the q-q plots comparing DCPD and breakdowns to q-q plots of uncorrelated data.

Fig. 5 (a)-(d) contain the q-q plots for DCPD and breakdowns of LDPE, PI, PEEK, and BOPP, respectively. Plots are shown with room temperature data except Fig. 5 (c) for PEEK. PEEK tests were spread across several temperatures and doses. For PEEK, data from tests done at 360 K are shown. The DCDP count accuracy for the few room temperature tests was reduced due to significant field-enhanced conductivity and erratic current traces convoluted with the DCPD. Due to the difficulty of counting DCPD between the last baseline current and breakdown, we re-plot the q-q plots normalized to the maximum field for value in the insets [25]. Clear outliers in measured breakdown field values, attributed to extrinsic sample damage or instrumentation issues identified above, were neglected in the statistical analysis presented in this study; this represented less than 1% of more than 330 measured step-up tests considered here [36].

To contrast the q-q plots in Fig. 5, observe the q-q plots of arbitrary uncorrelated data in Fig. 6. Fig. 6 (a) compares vacuum chamber pressure and sample thickness from the LDPE room temperature data. Fig. 6 (b) compares the DCPD events from LDPE to the measured sample thicknesses of PI. Unlike the q-q plots in Fig. 5, these are clearly not linear, indicating that the variables chosen are not correlated, as expected.

It is clear from Fig. 5 that the DCPD and breakdowns are related for each of the polymers studied. Except for PI, the normalized q-q plots suggest that not only are the underlying distribution functions of DCPD and breakdowns correlated, they are nearly identical. To show the predictive power of this method, Fig. 7 is a q-q plot comparing the DCPD from 5 step-up runs of LDPE to 14 breakdowns from different tests from the same batch of material. Unlike the plots in Fig. 5, the DCPD used are not from the same runs as the breakdowns to which they are compared. Although there is a single outlier, this exercise strongly suggests that this relationship based on a fundamental underlying relationship between a material's tendency to exhibit DCPD and the likelihood of dielectric breakdown.

4 PHYSICAL INTERPRETATION OF DCPD AND DIELECTRIC BREAKDOWN

The non-parametric comparisons between DCPD and dielectric breakdown offered in the previous section clearly demonstrate that DCPD and breakdown are related, however, this was shown without offering any insight into the physical mechanisms for the connection between them. While that is satisfactory for justifying a heuristic approach to accelerating material breakdown characterization via DCPD, a physical model would add conceptual support to what has been shown empirically. In this section, we outline a physical mechanism for DCPD in context of a defect-driven thermodynamic model of breakdown, together with some experimental evidence for the model.

The statistical significance of this correlation between DCPD and breakdown supports the notion that DCPD and breakdown have the same—or at least closely related—physical origins. Physics-based models of breakdown are centered in an understanding of the spatial and energetic distributions of defects in the dielectric materials, the occupation of those defects, and the mechanisms and rates of charge migration from one defect to another.

4.1 DUAL-DEFECT MODEL

In previous work, we have outlined a dual-defect driven model of dielectric breakdown [10]. This model extends the well-known Crine mean field model that describes the likelihood of breakdown as a function of mean defect energy ΔG_{def}, uniform defect density N_{def}, and temperature T [42-45]. The dual-defect model we propose considers two defect species: (i) high-energy chemical defects, such as dangling bonds and (ii) low-energy physical defects, such as a kink in a polymer chain [10]. High-energy defects have a negligible repair rate, even at high temperatures; however, low-energy defects can have a significant repair rate which increases with increasing temperature. Similar notions have been proposed by other authors [46, 47]. In its initial incarnation, the dual-defect model—like the Crine model—

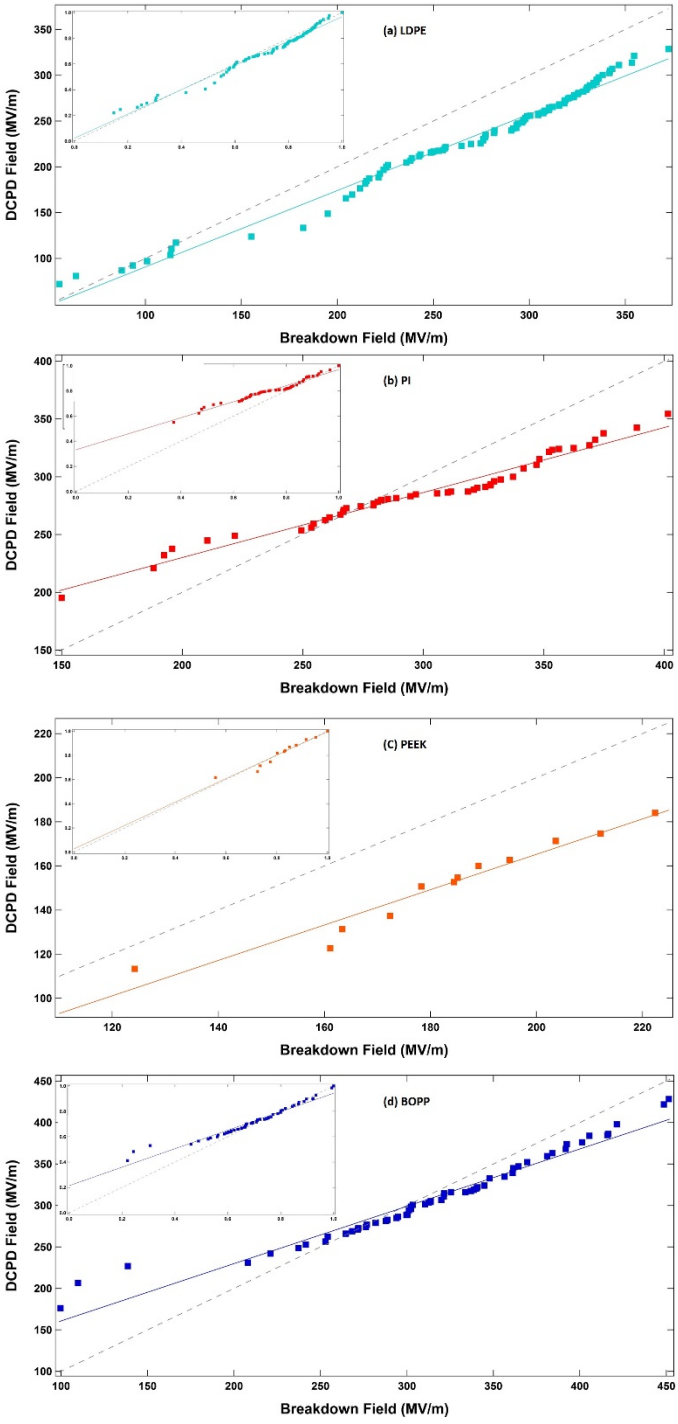

Figure 5. Quantile-Quantile plots of DCPD and dielectric breakdowns with linear fits. Dashed black lines are unity slope for reference. Insets are normalized to the maximum field for each data type. (a) LDPE (b) PI (c) PEEK (d) BOPP.

assumes mean defect energies ΔG_{def}^{HI} and ΔG_{def}^{LO} and uniform defect densities N_{def}^{HI} and N_{def}^{LO}.

The dual defect model predicts that the total probability of breakdown due to both defect contributions. P_{def}^{Tot}, as a function of wait time Δt at a given electric field F, and temperature T for high HI and low LO energy defects is

$$P_{def}^{Tot}(\Delta t, F, T) = \sum_{i=HI,LO} P_{def}^{i} = \left(\frac{2k_b T}{h/\Delta t}\right) \sum_{i=HI,LO} \exp\left[\frac{-\Delta G_{def}^{i}}{k_b T}\right] \sinh\left[\frac{\varepsilon_o \varepsilon_r F^2}{2 N_{def}^{i} k_B T}\right] \quad (2)$$

where k_b is Boltzmann's constant, h is Planck's constant, ε_o is the permittivity of free space, and ε_r is the relative permittivity. The dual-defect model has been shown to fit breakdown data in LDPE and PI better than the single defect Crine model for both voltage step-up to breakdown and static voltage endurance time test configurations [10, 36].

We propose that a candidate physical mechanism for DCPD is that they are cascades of charge, which cause sufficient heating to locally anneal low-energy defects needed for further propagation, quenching the discharge before it leads to total dielectric breakdown. Dielectric breakdown occurs when the annealing mechanism is insufficient to stop the cascade from growing.

Alternately, one might think of a lattice of defect sites with the density of high-energy defects near, but below, the percolation threshold. While high-energy defects are largely independent of temperature, their density could be increased through radiation damage or through prolonged exposure to F field stress (The latter is the essence of endurance time tests.). Additional low energy defects could act in concert with the high-energy defects to complete a percolation path. However, these low energy defects would have small average lifetime and be much more dependent on T. The generation of such defects would follow an Arrhenius behavior, much like the generation of phonons in a periodic crystalline lattice [48] or the temperature dependence of photon emission in cathodoluminescence [49]. Thus, completion of the percolation path would be expected to increase with increasing T due to defect recovery, but would be transient.

Future work will outline the differential equations governing the creation and annihilation rates and equilibrium behavior of recoverable defects. More sophisticated models will consider both spatial and energetic distributions of these defects and even distributions that change with temperature, dose, and stress imposed on the materials while under field *F*, or the time *t* a material is exposed to such stress.

4.2 MEASUREMENTS VERSUS TEMPERATURE AND DOSE

As presented here, the extension of the dual-defect breakdown model is only conceptual. A detailed mathematical

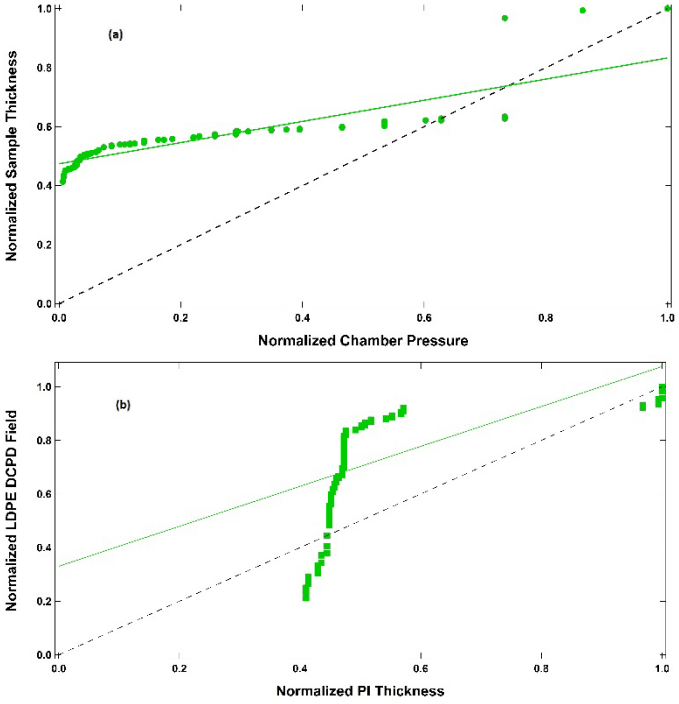

Figure 6. Quantile-Quantile plots of uncorrelated data with linear fit. Dashed black line is unity slope for reference. (a) Sample thickness and chamber pressure from a set of breakdown tests. (b) DCPD in LDPE tests and PI sample thickness.

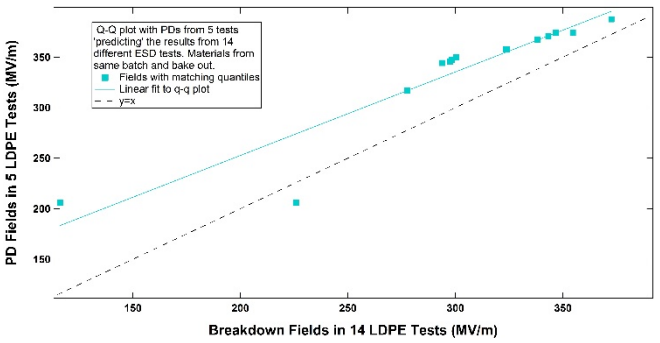

Figure 7. Quantile-Quantile plots of DCPD and breakdowns from different tests with linear fit. Dashed black line is unity slope for reference.

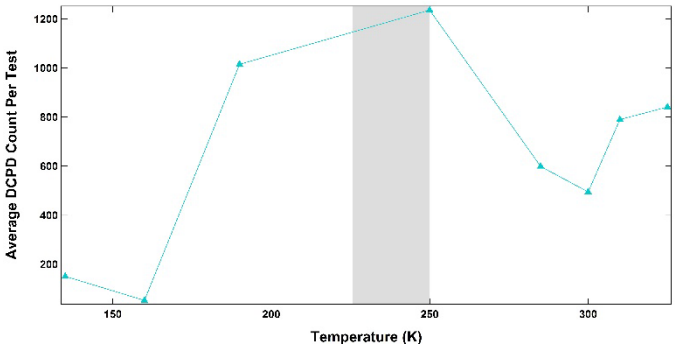

Figure 8. Average DCPD count per test versus temperature in LDPE. Glass transition range shown for reference.

description of DCPD in the context of this breakdown model will be published in a future paper dedicated to the topic. For the purposes of the current paper, we note in (2) that the probability of breakdown, and therefore DCPD, should depend significantly on temperature and or changes the defect density that could depend on both temperature and radiation dose. We include some preliminary data for such dependence to show how that it, at least qualitatively, agrees with the general extended model [50].

Fig. 8 shows the average DCPD count per run versus temperature for LDPE. We see that the discretized DCPD count is significantly reduced at the lowest temperatures. The large discontinuity above ~250 K where the count drops and then begins to increase again may be due to the glass transition in LDPE at about that temperature [10, 51].

Fig. 9 (a) shows the average DCPD count per run versus temperature and irradiated dose for PEEK [50]. Like with LDPE, there is a trend to increased DCPD with increasing temperature. The DCPD per run also increase significantly with increased dose. (There is a single outlier at the highest radiation (75 MRad) and temperature (~360 K).)

Fig. 9 (b) shows the breakdown electric field versus temperature and dose from the same tests of PEEK. Note the similarities in the overall dose and temperature dependence between breakdown voltage and DCPD count.

These measurements show that DCDP depend on both temperature and defect density through radiation dose. As suggested by the qualitative discussion of the dual-defect model above, higher temperatures lead to more low-energy defects and increased likelihood of completing a percolation network leading to more DCPD. Alternately, increased dose increases defect density, and thereby reduces the density of low-energy defects required to complete the percolation network. The temperature and dose trends in Fig. 8 and Fig. 9 (a) are qualitatively consistent with aspects of the dual–defect model. Although additional tests are needed to enhance the comparison, the limited breakdown data at different temperatures and doses indicate similar trends in breakdowns. Q-q analyses for the tests at various temperatures and doses described in this section are quite sparse given the limited breakdowns at each unique combination of dose and temperature. Nevertheless, these appeared to show good correlation, except for PEEK samples having been exposed to 75 Mrad of beta radiation.

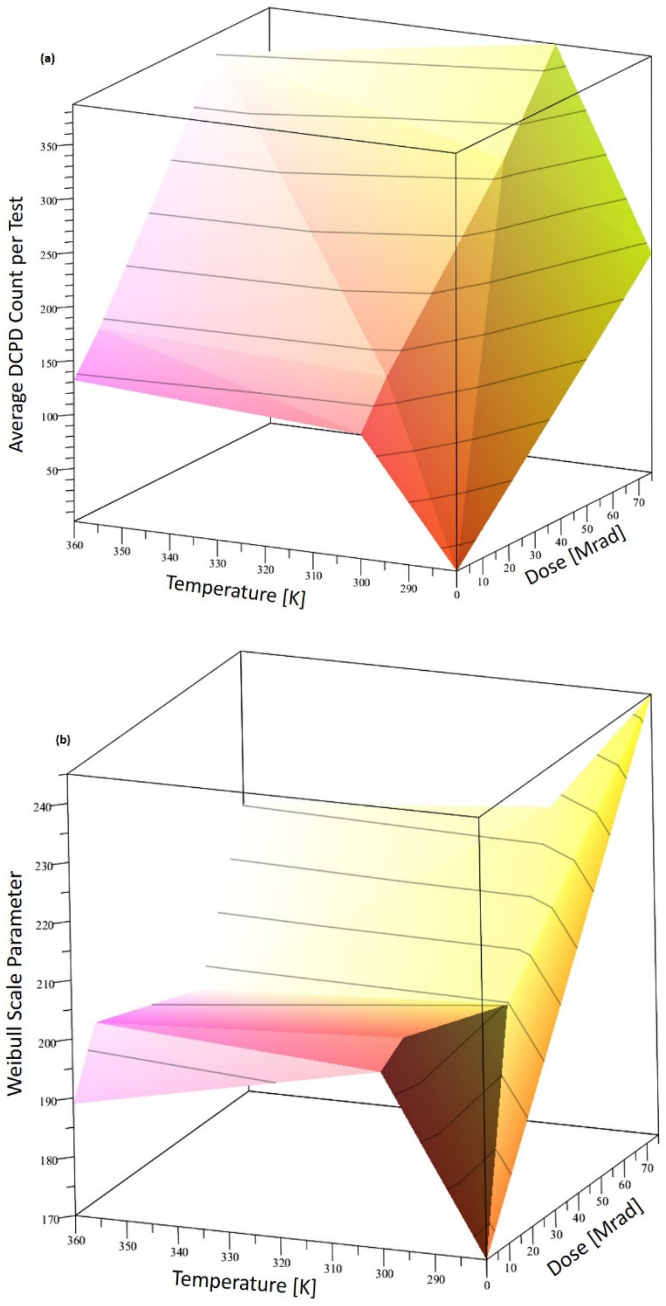

Figure 9. (a) Average DCPD count per run versus temperature and dose for PEEK. (b) Nominal breakdown electric field versus temperature and dose for PEEK. Note the similarities in temperature and dose dependence.

5 CONCLUSION

DC voltage step-up to breakdown tests with sufficiently slow ramp rates and constant leakage current monitoring exhibit numerous DCPD before breakdown. Data for four common polymers presented here support this; additional lower resolution studies of other polymers and some glass materials exhibit similar phenomena and trends. Careful analysis of several hundred step-up to breakdown tests together with high time resolution in-line and RF PD measurements provide compelling evidence that observed DCPD are not erroneous noise, not related to other transient phenomena, and not expected to be readily observed with more common step-up to breakdown test methods. Quantile-quantile plots of the cumulative distributions of DCPD and breakdown events show that these two phenomena are closely correlated. Given that many DCPD are observed during a single breakdown test, using the DCPD distribution, especially the inception field, as an estimate for the distribution of breakdowns, the characterization of HVDC insulating material can be greatly expedited. With further development, the correlation of DCPD and breakdown could be applied to condition monitoring diagnostic techniques similar to those used to detect and localize ACPD [47].

The temperature and radiation dependence of DCPD supports the notion that DCPD can be explained in context of recoverable defects in a dual-defect thermodynamic dielectric breakdown model.

ACKNOWLEDGMENT

The work of A. Andersen was supported by the NASA Space Technology Research Fellowship. We acknowledge John Stevens of Utah State University and Dave Brown of Brigham Young University-Idaho for their insightful discussions. Current and previous members of the Utah State University Materials Physics Group, including Greg Wilson, Tyler Kippen, Krysta Moser, Charles Sim, Dan Arnfield and Anthony Thomas, provided invaluable assistance with instrumentation and experiments.

REFERENCES

[1] A. Cavallini, P. Morshuis, and G. C. Montanari, "Call for papers: High Voltage Direct Current (HVDC) insulation and diagnostics," *IEEE Transactions on Dielectrics and Electrical Insulation*, vol. 23, pp. 3779-3779, 2016.

[2] E. Corr, W. H. Siew, and W. Zhao, "Long term testing and analysis of dielectric samples under DC excitation," in *2016 IEEE Electrical Insulation Conference (EIC)*, 2016, pp. 484-487.

[3] J. P. Crine, "On the interpretation of some electrical aging and relaxation phenomena in solid dielectrics," *Dielectrics and Electrical Insulation, IEEE Transactions on*, vol. 12, pp. 1089-1107, 2005.

[4] T. T. N. Vu, G. Teyssedre, B. Vissouvanadin, S. Le Roy, C. Laurent, M. Mammeri, *et al.*, "Electric field profile measurement and modeling in multi-dielectrics for HVDC application," in *Solid Dielectrics (ICSD), 2013 IEEE International Conference on*, 2013, pp. 413-416.

[5] P. Trnka, M. Sirucek, M. Svoboda, and J. Soucek, "Condition-based maintenance of high-voltage machines-a practical application to electrical insulation," *Electrical Insulation Magazine, IEEE*, vol. 30, pp. 32-38, 2014.

[6] T. Czaszejko, "High-voltage testing fundamentals: a cable testing perspective," *Electrical Insulation Magazine, IEEE*, vol. 30, pp. 7-13, 2014.

[7] A. Andersen, J. Dennison, and K. Moser, "Perspectives on the Distributions of ESD Breakdowns for Spacecraft Charging Applications," *IEEE Tran. Plasma Science*. 2017, vol. 45, pp. 2031-2035, 2017.

[8] ASTM, "Standard Test Method for Dielectric Breakdown Voltage and Dielectric Strength of Solid Electrical Insulating Materials Under Direct-Voltage Stress," vol. D3755-14, ed, 2014.

[9] ASTM, "Standard Test Method for Electric Breakdown Voltage and Dielectric Strength of Solid Electrical Insulating Materials at Commercial Power Frequencies," vol. D149-97a, ed, 2004.

[10] A. Andersen, J. R. Dennison, A. M. Sim, and C. Sim, "Measurements of Endurance Time for Electrostatic Discharge of Spacecraft Materials: A Defect-Driven Dynamic Model," *Plasma Science, IEEE Transactions on*, vol. 43, pp. 2941-2953, 2015.

[11] ASTM, "Standard Specification for Polymeric Resin Film for Electrical Insulation and Dielectric Applications," vol. D5213-12, ed, 2012.

[12] "Material Information-Polyethylene Low Density LDPE," Goodfellow, Ed., ed. Devon, PA, 2006.

[13] H. J. Wintle, "Conduction Processes in Polymers," in *Engineering Dielectrics-Volume IIA: Electrical Properties of Solid Insulating Materials: Molecular Structure and Electrical Behavior*. vol. IIA, R. Bartnikas, Ed., ed Philadelphia, PA: American Society for Testing and Materials, 1983.

[14] J. Brunson, "Measurement of charge decay time and resistivity of spacecraft insulators using charge storage method and application to theoretical modeling of charging behavior of insulators," *Physics. Vol. PhD, Utah State University, Logan, UT*, p. 215, 2009.

[15] A. Peacock, *Handbook of polyethylene: structures: properties, and applications*: CRC Press, 2000.

[16] "DuPont Kapton HN polyimide film, H-38479, Bulletin GS-96-7,," vol. document K-15345-1, DuPont, Ed., ed. Circleville, OH, USA, 2011.

[17] "Standard Price List for Polypropylene," Goodfellow, Ed., ed. Coraopolis, PA, 2017.

[18] "Standard Price List for Polyetheretherketone," Goodfellow, Ed., ed. Coraopolis, PA, 2016.

[19] A. Andersen and J. Dennison, "An Enhanced Operational Definition of Dielectric Breakdown for DC Voltage Step-up Tests," in *Conference on Electrical Insulation and Dielectric Phenomena—(CEIDP)*, Fort Worth, TX, 2017.

[20] J. Dekany, A. M. Sim, J. Brunson, and J. R. Dennison, "Electron Transport Models and Precision Measurements with the Constant Voltage Conductivity Method," *IEEE Transactions on Plasma Science*, vol. 41, p. 12, 2013.

[21] "Low Level Measurements Handbook - 7th Edition," Keithley, Ed., 7 ed, 2016.

[22] J. Dennison, J. C. Gillespie, A. Andersen, A. E. Jensen, G. Wilson, J. Dekany, *et al.*, "Synergistic Models of Electron Emission and Transport Measurements of Disordered SiO2," in *14th Spacecraft Charging Technology Conference*, Noordwijk, The Netherlands, 2016.

[23] K. Moser, A. Andersen, and J. Dennison, "Dependence of Electrostatic Field Strength on Voltage Ramp Rate for Spacecraft Materials," *IEEE Tran. Plasma Science*, vol. 45, pp. 2036-2039, 2017.

[24] A. Andersen and J. Dennison, "Pre-breakdown Arcing and Electrostatic Discharge in Dielectrics under High DC Electric Field Stress," *2014 Annual Report Conference on Electrical Insulation and Dielectric Phenomena*, pp. 63-66, 2014.

[25] A. Andersen and J. R. Dennison, "Pre-breakdown arcing as proxy for DC dielectric breakdown testing of polymeric insulators," in *Electrical Insulation and Dielectric Phenomena (CEIDP), 2015 IEEE Conference on*, 2015, pp. 574-577.

[26] A. H. El-Hag, N. Qaddoumi, R. Mourtada, E. A. Murawwi, A. Nimer, K. AlMazam, *et al.*, "Multi-purpose RF antenna for partial discharge and oil quality monitoring," in *2013 3rd International Conference on Electric Power and Energy Conversion Systems*, 2013, pp. 1-5.

[27] J. Liu, G. Zhang, J. Dong, and J. Wang, "Study on miniaturized UHF antennas for partial discharge detection in high-voltage electrical equipment," *Sensors*, vol. 15, pp. 29434-29451, 2015.

[28] Z. Tang, C. Li, X. Cheng, W. Wang, J. Li, and J. Li, "Partial discharge location in power transformers using wideband RF detection," *IEEE Transactions on Dielectrics and Electrical Insulation*, vol. 13, pp. 1193-1199, 2006.

[29] P. H. F. Morshuis and J. J. Smit, "Partial discharges at DC voltage: their mechanism, detection and analysis," *IEEE Transactions on Dielectrics and Electrical Insulation*, vol. 12, pp. 328-340, 2005.

[30] I. Rytöluoto, K. Lahti, M. Karttunen, and M. Koponen, "Large-area dielectric breakdown performance of polymer films - part i: measurement method evaluation and statistical considerations on area-dependence," *Dielectrics and Electrical Insulation, IEEE Transactions on*, vol. 22, pp. 689-700, 2015.

[31] H. Wang, P. Zongren, L. Naiyi, Z. Shiling, G. Zihao, and Z. SiYu, "Transient electric field calculation of UHV GIS spacer under lightning impulse," in *Electrical Insulation and Dielectric Phenomena (CEIDP), 2014 IEEE Conference on*, 2014, pp. 542-545.

[32] L. A. Dissado and J. C. Fothergill, *Electrical Degradation and Breakdown in Polymers*. London, UK: The Institution of Engineering and Technology, 1992.

[33] C. Chauvet and C. Laurent, "Weibull statistics in short-term dielectric breakdown of thin polyethylene films," *Electrical Insulation, IEEE Transactions on*, vol. 28, pp. 18-29, 1993.

[34] L. Zavattoni, R. Hanna, O. Lesaint, and O. Gallot-Lavallee, "Dark current measurements in pressurized SF6: Influence of relative humidity and temperature," in *Electrical Insulation and Dielectric Phenomena (CEIDP), 2014 IEEE Conference on*, 2014, pp. 23-26.

[35] L. Arevalo and W. Dong, "Effect of high dielectric protrusions on the breakdown phenomena of large electrodes under positive switching impulses," in *Electrical Insulation and Dielectric Phenomena (CEIDP), 2014 IEEE Conference on*, 2014, pp. 51-54.

[36] A. Andersen and J. R. Dennison, "Mixed Weibull distribution model of DC dielectric breakdowns with dual defect modes," in *Electrical Insulation and Dielectric Phenomena (CEIDP), 2015 IEEE Conference on*, 2015, pp. 570-573.

[37] C. M. Kerwien, D. L. Malandro, and J. R. Broomall, "Large area DC dielectric breakdown voltage measurement of BOPP and PTFE thin films," in *Electrical Insulation and Dielectric Phenomena (CEIDP), 2016 IEEE Conference on*, 2016, pp. 486-489.

[38] D. C. Hoaglin, "Using quantiles to study shape," *Exploring data tables, trends, and shapes*, pp. 417-460, 1985.

[39] J. H. Einmahl and I. W. McKeague, "Confidence tubes for multiple quantile plots via empirical likelihood," *The Annals of Statistics*, vol. 27, pp. 1348-1367, 1999.

[40] W. A. Rosenkrantz, "Confidence bands for quantile functions: A parametric and graphic alternative for testing goodness of fit," *The American Statistician*, vol. 54, pp. 185-190, 2000.

[41] J. Valeinis, E. Cers, and J. Cielens, "Two-sample problems in statistical data modelling," *Mathematical modelling and analysis*, vol. 15, pp. 137-151, 2010.

[42] J. P. Crine, "A molecular model for the electrical aging of XLPE," in *2007 Annual Report - Conference on Electrical Insulation and Dielectric Phenomena*, 2007, pp. 608-610.

[43] J.-L. Parpal, J.-P. Crine, and C. Dang, "Electrical aging of extruded dielectric cables. A physical model," *IEEE transactions on dielectrics and electrical insulation*, vol. 4, pp. 197-209, 1997.

[44] J.-P. Crine, J.-L. Parpal, and C. Dang, "A new approach to the electric aging of dielectrics," in *Electrical Insulation and Dielectric Phenomena, 1989. Annual Report., Conference on*, 1989, pp. 161-167.

[45] J. P. Crine, "Origin and Nature of the Activated Parameters in the Electrical Aging Equation," in *2008 Annual Report Conference on Electrical Insulation and Dielectric Phenomena*, 2008, pp. 99-102.

[46] K. C. Kao, *Dielectric phenomena in solids*: Academic press, 2004.

[47] H. Cho, Y. C. Kim, S. O. Kim, and I. J. Chung, "Persistence length calculation from light scattering and intrinsic viscosity of dilute semiflexible polyimide solutions with different degree of imidization," *Korea-Australia Rheology Journal*, vol. 12, pp. 69-76, 2000.

[48] C. Kittel, *Introduction to solid state*: John Wiley & Sons, 1966.

[49] A. E. Jensen and J. R. Dennison, "Defects Density of States Model of Cathodoluminescent Intensity and Spectra of Disordered SiO2," *IEEE Transactions on Plasma Science*, vol. 43, pp. 2925-2932, 2015.

[50] T. Kippen, A. Andersen, and J.R. Dennison, “Temperature Dependency of Electrostatic Breakdown in LDPE and PEEK,” *American Physical Society Four Corner Section Meeting*, New Mexico State University, Las Cruses, NM, October 21-22, 2016.

[51] J.R. Dennison and J. Brunson, “Temperature and Electric Field Dependence of Conduction in Low-Density Polyethylene,” *IEEE Transaction on Plasma Science*, vol. 36, pp. 2246-2252, 2008.

Allen Andersen (GS’15) is currently a graduate student at Utah State University in Logan, UT pursing a PhD in physics. He received a BS degree in physics from BYU-Idaho in 2012. He has worked with the Materials Physics Group for five years on electron transport measurements, electrostatic discharge tests, and electron emission measurements related to spacecraft charging. IEEE Graduate Student Member.

JR Dennison (M’12) received the B.S. degree in physics from Appalachian State University, Boone, NC, in 1980, and the M.S. and Ph.D. degrees in physics from Virginia Tech, Blacksburg, in 1983 and 1985, respectively. He was a Research Associate with the University of Missouri—Columbia before moving to Utah State University (USU), Logan, in 1988. He is currently a Professor of physics at USU, where he leads the Materials Physics Group. He has worked in the area of electron scattering for his entire career and has focused on the electron emission and conductivity of materials related to spacecraft charging for the last two decades. IEEE member.